frontiers in Materials

ORIGINAL RESEARCH
published: 12 May 2020
doi: 10.3389/fmats.2020.00092

Tensile Properties and Impact Toughness of $AlCo_xCrFeNi_{3.1-x}$ (x = 0.4, 1) High-Entropy Alloys

*Lu Zhang and Yong Zhang**

Beijing Advanced Innovation Center of Materials Genome Engineering, State Key Laboratory for Advanced Metals and Materials, University of Science and Technology Beijing, Beijing, China

In this work, $AlCo_xCrFeNi_{3.1-x}$ (x = 0.4, 1) high-entropy alloys (HEAs) were investigated. The effects of different Co and Ni content (both of which are FCC stabilizers with similar atomic radii) on the microstructure and mechanical properties of the system were studied with the goal of improving the cost-effectiveness of the alloys. $AlCo_{0·4}CrFeNi_{2·7}$ and $AlCoCrFeNi_{2·1}$ were prepared via vacuum induction melting. X-ray diffraction and scanning electron microscope results demonstrated that an FCC+B2 structure formed. Additionally, tensile tests at room temperature and impact tests at 77, 200, and 298 K were also carried out. From the results, it could be determined that the tensile properties of the tested samples were similar. The impact toughness of $AlCo_{0·4}CrFeNi_{2·7}$ with a V-notch was 21.77 J at 298 K, and this was more than three times larger than that of $AlCoCrFeNi_{2·1}$. Compared with the $Al_{0·3}CoCrFeNi$ and $Al_{0·1}CoCrFeNi$ FCC structured HEAs, $AlCo_xCrFeNi_{3.1-x}$ alloys showed low impact toughness but had a high yield strength.

Keywords: high-entropy alloys, eutectic, microstructure, tensile properties, impact toughness

OPEN ACCESS

Edited by:
Yanzhong Tian,
Northeastern University, China

Reviewed by:
Fu-Fa Wu,
Liaoning University of Technology, China
Xinwang Liu,
Huazhong University of Science and Technology, China

***Correspondence:**
Yong Zhang
drzhangy@ustb.edu.cn

Specialty section:
This article was submitted to Structural Materials, a section of the journal Frontiers in Materials

Received: *31 January 2020*
Accepted: *25 March 2020*
Published: *12 May 2020*

Citation:
Zhang L and Zhang Y (2020) Tensile Properties and Impact Toughness of $AlCo_xCrFeNi_{3.1-x}$ (x = 0.4, 1) High-Entropy Alloys. Front. Mater. 7:92. doi: 10.3389/fmats.2020.00092

INTRODUCTION

The development of materials tends to increase the complexity of their constituent components and increases entropy. High-entropy alloys (HEAs) are a type of advanced material that were first reported in 2004 (Yeh et al., 2004). Conventional materials are generally based on one or two elements, with further elemental doping being used to tune their properties. HEAs overcome the limitations of their constituent components and generally refer to a class of alloys that contain >5 elements (between 5–35 at.%) that tend to form solid solution phases (Yeh et al., 2004). For example, this class of materials includes $Al_{0·3}CoCrFeNi$ alloys with a face-centered-cubic (FCC) structure (Li et al., 2017), AlCoCrFeNi alloys with a body-centered-cubic (BCC) structure (Manzoni et al., 2013), and GdHoLaTbY alloys with a hexagonal-close-packing (HCP) structure (Zhao et al., 2016).

Over the last few years, the HEA family has gradually expanded and second-generation HEAs have now been developed. These materials contain >4 main elements and form two-phase or multi-phase structures (Zhang W. et al., 2018), such as $AlCoCrFeNi_{2·1}$ eutectic HEAs (Lu et al., 2014) and $Fe_{50}Mn_{30}Cr_{10}Co_{10}$ TRIP HEAs (Li et al., 2016). Research in the HEAs field is not limited to three-dimensional bulk alloys, but also extends to thin-films (two-dimensional) and fibers (one-dimensional) (Zhang, 2019). Because of the solid solution strengthening effect, HEAs exhibit excellent properties that surpass other conventional alloys, such as high hardness and strength, excellent corrosion resistance, good wear resistance, and excellent high temperature resistance (Zhang, 2019).

Casting is an important and widely used technique for almost all engineering materials. Because of the compositional complexity of HEAs, as-cast HEAs with excellent properties can be obtained via tuning of the composition. For instance, Liu et al. (2018) added C to CrFeCoNi HEAs to obtain refined grains. Lv et al. (2019) used $Fe_{50}Mn_{30}Co_{10}Cr_{10}$ TRIP (transformation-induced plasticity) HEAs as a matrix with added C and Mo to refine the equiaxed crystal grains and increase deformation twins, which resulted in improvement of the tensile properties. Furthermore, $Fe_{50}Mn_{30}Co_{10}Cr_{10}C_2Mo$ displayed a high tensile strength (∼658 MPa) and plasticity (∼89.8%). In addition, an as-cast $AlCoCrFeNi_{2\cdot1}$ eutectic high-entropy alloy (EHEA) was prepared by Lu et al. (2014) attracting broad research attention. Because of its eutectic structure (FCC+B2), this alloy has good casting fluidity and excellent mechanical properties.

In previous studies, $AlCoCrFeNi_{2\cdot1}$ HEA demonstrated numerous excellent properties because of its eutectic structure. However, this alloy incorporates cobalt, which is expensive, and this has limited the wide application of $AlCoCrFeNi_{2\cdot1}$. In the present study, the amount of Co was reduced and partially replaced by the cheaper element, Ni. The atomic radii of Co and Ni are similar and the contents of the other three elements Al, Cr, and Fe were held constant; hence, the atomic size difference of the modified system was unchanged. Ke et al. (2006) also found that Co and Ni usually functioned as "FCC stabilizers"; therefore, substitution of Co by Ni would not have a significant effect on the phase composition of the alloy system. For the above reasons, the $AlCo_xCrFeNi_{3.1-x}$ (x = 1, 0.4) system was studied, i.e., the $AlCoCrFeNi_{2\cdot1}$ and $AlCo_{0\cdot4}CrFeNi_{2\cdot7}$ alloys (abbreviated as Ni2.1 and Ni2.7, respectively). The goal of this work was to study the effects of changes in the Co and Ni content on the properties of the system.

EXPERIMENTAL

$AlCoCrFeNi_{2\cdot1}$ and $AlCo_{0\cdot4}CrFeNi_{2\cdot7}$ were made via vacuum induction melting, with high purity elements (Al, Co, Ni: 99.9 wt.%; Cr, Fe: 99.5–99.6 wt.%). All the raw materials were placed in a ZrO_2 crucible, heated to 600°C, and held for 1 h to remove water vapor. The pouring temperature was set at 1500°C and the temperature was monitored with an absolute accuracy of ±2°C using an IRTM-2CK infrared pyrometer. Approximately 2.5 kg of metal was melted, superheated, and poured into a high-purity graphite crucible with a length of 220 mm, an upper inner diameter of 62 mm and a bottom inner diameter of 50 mm. In all cases, the furnace chamber was first evacuated to 6×10^{-2} Pa and then backfilled with high-purity argon gas to reach 0.06 MPa.

The crystal structure was identified via X-ray diffraction (XRD) (D8-ADVANCE, Karlsruhe, Germany) with Cu Kα irradiation (40 kV, 300 mA) at a scanning speed of 2°/min. The scanning range was set between 20–100°. For microstructural characterization, the ingots were sectioned, ground, polished, and etched with marble solution ($CuSO_4$:HCl:H_2O = 1:5:5). Then, they were observed using an optical microscope (OM) (Axio imager A2m, Jena, Germany) and a field-emission scanning electron microscope (SEM) (ZEISS SUPRA 55, Jena, Germany), equipped with an X-ray energy spectrometer (EDS) (ZEISS SUPRA 55, Jena, Germany).

The mechanical properties were studied in terms of the tensile and impact properties. Tensile testing was carried out on a CMT Model 4305 Universal Electronic Tester at room temperature with a strain rate of 0.5 mm/s. A non-standard sample size was used, as shown in **Figure 1A**. The impact tests were conducted on an ASTM standard E-23 setup (size: 10 mm × 10 mm × 55 mm; with a 2 mm deep, V-notch or U-notch at the center, as shown in **Figure 1B**) at T = 298, 200, and 77 K on a Tinius Olsen impact tester with 450 J impact energy.

RESULTS

Microstructure

Macroscopic, OM, and SEM images of the Ni2.7 and Ni2.1 alloys are shown in the **Figure 2**. **Figure 2A** shows the macroscopic picture of bulk Ni2.1 and Ni2.7 ingots. **Figures 2B,C** are OM images of Ni2.7 and Ni2.1, respectively. It can be clearly seen that the Ni2.1 alloy forms a uniform lamella structure that is consistent with the characteristics of eutectic alloys. The Ni2.7 alloy has many large primary phases (white part in the **Figure 2B**). **Figures 2D,E** show SEM images of the two alloys. The coupled two phase growth displays a clear compositional contrast, with the regions marked as A (A_1 and A_2) in **Figures 2D,E** being rich in Co, Cr, and Fe, while the regions marked as B (B_1 and B_2) were rich in Al and Ni (detailed compositional information given in **Table 1**). In the Ni2.7 alloy, large A_1 regions can be observed, and the other regions were filled by an A_1/B_1 eutectic structure. In the Ni2.1 alloy, the formation of uniform and fine A_2/B_2 lamella could be observed.

Figure 3 shows XRD patterns of the alloys. It can be seen that both FCC and B2 structures exist inside the two alloys. Therefore, a change in the ratio of Co and Ni did not have much influence on phase formation in this system.

Compositional analysis of the alloys was carried out and the results are summarized in **Table 1**. The actual composition was very close to the nominal composition, indicating that there was very little volatilization of the elements. Obvious elemental segregation occurred in the A and B areas. By combining the previous XRD analysis and experimental results from prior literature, it can be determined that the A region (A_1 and A_2) is the FeCoCr-rich phase, i.e., the FCC phase, and the B region (B_1 and B_2) is the AlNi-rich phase, which is the B2 phase. Therefore, the Ni2.1 alloy forms a FeCoCr/AlNi eutectic phase, and the Ni2.7 alloy was composed of a FeCoCr primary phase and the FeCoCr/AlNi eutectic structure; in other words, there was more FeCoCr-rich (FCC) phase in the Ni2.7 alloy.

Tensile Properties

The tensile stress-strain curves of these two alloys at room temperature are shown in the **Figure 4**. There was no obvious yielding stage in the tensile curve, so $\sigma_{0\cdot2}$ was chosen as the yield strength. The tensile properties of the Ni2.7 and Ni2.1 alloys are similar to each other at room temperature. The yield strength

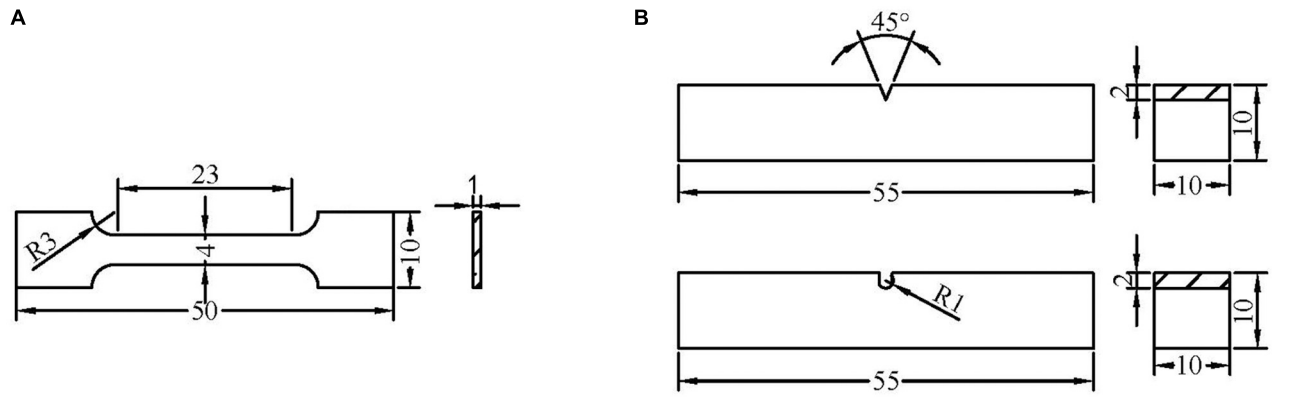

FIGURE 1 | Schematics of the samples for **(A)** tensile tests and **(B)** impact tests.

was ∼540 MPa, while the fracture strength and elongation were 941.1 MPa, 8.5%, and 1068.8 MPa, 8.2%, respectively.

The fracture surface morphology of the Ni2.1 and Ni2.7 alloys are shown in **Figure 5**. Both the fracture surfaces mainly exhibited a trench-like microstructure, which was caused by the FCC/B2 eutectic structure. The bottom of the trench was smooth, and the edge was a bright white line composed of dimples. **Figures 5A,B** were nearly similar. There were more bright lines for the Ni2.7 alloy than for the Ni2.1 alloy, which is consistent with the increased elongation of the Ni2.7 alloy.

Impact Properties

Figure 6 shows the impact energy of these two alloys with V- and U-notches at 298, 200, and 77 K. The impact energies reduced with decreasing temperature for both the U-notch and V-notch samples. Additionally, all the samples completely broke into two pieces, suggesting little resistance against crack propagation.

For the same alloy, the impact energy of the U-notch samples was slightly higher than for the V-notch samples. The V-notch was sharp and stress concentrated at the center, which made plastic deformation difficult and most of the impact energy was spent in crack propagation. However, the impact energy in the U-notch samples was primarily expended on crack formation. This resulted in the impact energy of the V-notch samples being lower.

For the different alloys, the impact energy of the Ni2.7 alloy was significantly higher than that of the Ni2.1 alloy. Since the V-notch sample is used more widely, it was the subject of the subsequent analyses unless otherwise stated. For the Ni2.7 alloy, the impact energy at room temperature (298 K) was 21.77 J. When the temperature declined to 77 K, the impact energy also reduced to 8.14 J. The impact energy of the Ni2.1 alloy did not exceed 10 J and was ∼3.76 J at 77 K, and it finally reached 6.33 J at room temperature. The microscopic images of the impact fractures display similar features as the tensile fractures, i.e., a trench-like microstructure. The difference being that more white lines were present in the Ni2.1 alloy and it clearly showed cleavage fracture.

DISCUSSION

Phase Formation

Based on the various parameters that influence the phase formation of HEAs, several thermodynamic parameters have been proposed from experimental results and theoretical calculations. Solid solutions can be formed if these parameters are distributed in a certain range. Among these parameters, the atomic size difference (δ), mixing enthalpy (ΔH_{mix}), and mixing entropy (ΔS_{mix}) are the most widely used and they can be calculated as follows (Guo and Liu, 2011; Yang and Zhang, 2012; Zhang et al., 2014):

$$\delta = \sqrt{c_i \left(1 - \frac{r_i}{\bar{r}}\right)^2}, \tag{1}$$

$$\Delta H_{\text{mix}} = \sum_{i \neq j} 4 c_i c_j \Delta H_{ij}^{\text{mix}}, \tag{2}$$

$$\Delta S_{\text{mix}} = -R \sum c_i \ln c_i, \tag{3}$$

$$\Omega = \frac{T_m \Delta S_{\text{mix}}}{|\Delta H_{\text{mix}}|}, \tag{4}$$

where $\bar{r}$ is the average atomic radius of each constituent element, r_i is the atomic radius of the i-th element, $\Delta H_{ij}^{\text{mix}}$ is the mixed enthalpy of the i-th and j-th elements, R is the gas constant (R = 8.314 J·mol^{-1}·K^{-1}), and T_m is the melting temperature of the alloy.

Table 2 shows some of the thermodynamic factors of the Ni2.7 and Ni2.1 alloys. Because of the similar atomic radii of Co and Ni, adjusting the ratio of Co and Ni would not affect the δ of the system when the other element contents were kept constant. Compared with the Ni2.1 alloy, there was more Ni but less Co in the Ni2.7 alloy, which led to a smaller ΔS_{mix}. As shown in **Figure 7**, with the increasing entropy value, the properties of the alloy first increased and then decreased, while the trend in the cost was different (Zhang Y. et al., 2018). Hence, the cost-effective alloys are

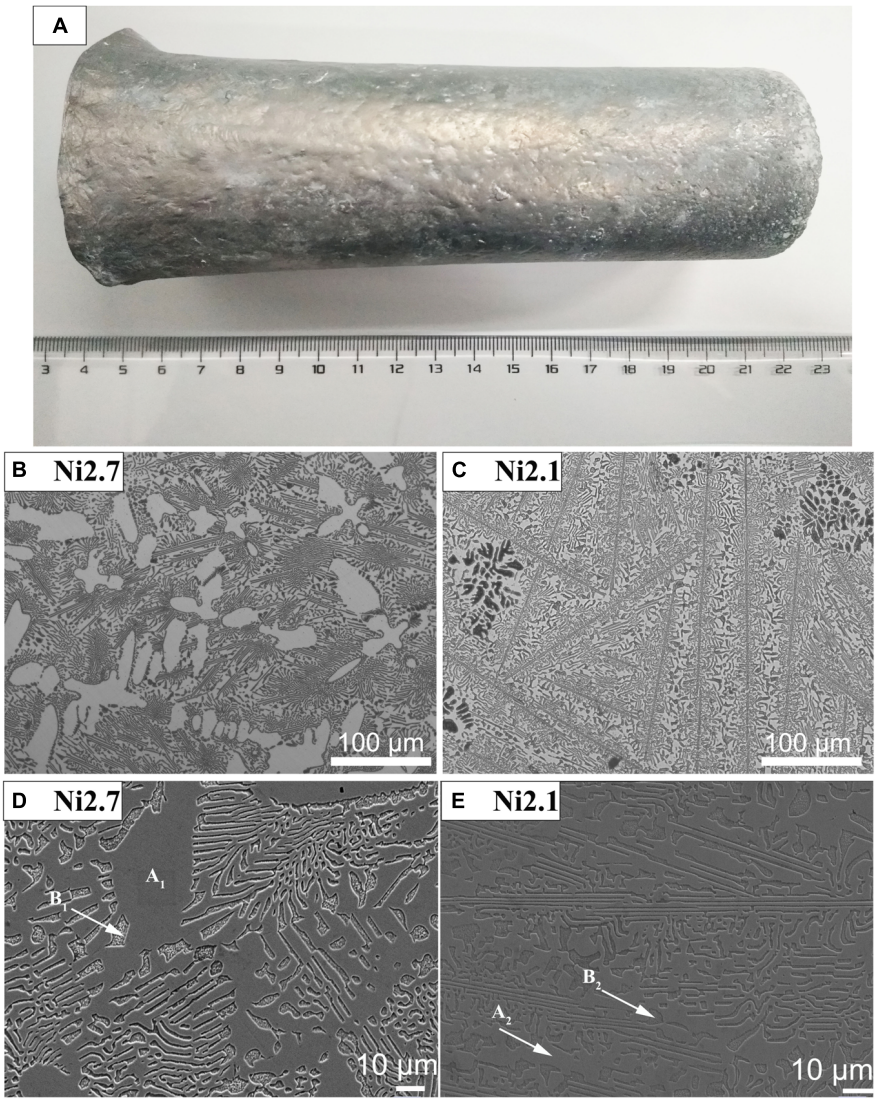

FIGURE 2 | Images of the $AlCo_xCrFeNi_{3.1-x}$ alloys obtained using different methods. **(A)** Macroscopic picture of the bulk ingot; **(B)** OM image of the Ni2.7 alloy; **(C)** OM image of the Ni2.1 alloy; **(D)** SEM image of the Ni2.7 alloy, and **(E)** SEM image of the Ni2.1 alloy.

most likely to appear within an entropy interval of 0.69–1.61 *R*. The ΔS_{mix} of the Ni2.7 and Ni2.1 alloys are plotted in **Figure 7**. It can be seen that both the ΔS_{mix} values are within this interval, so these two alloys could be highly cost-effective.

Guo and Liu (2011) provided a range for forming solid solutions: $-22 \leq \Delta H_{mix} \leq 7$ kJ/mol, $\delta \leq 8.5\%$, $11 \leq \Delta S_{mix} \leq 19.5$ J/(K mol). In addition, Zhang et al. (2014) proposed that the transition zone between the mixed ordered solid solution and disordered solid solution is: $-20 < \Delta H_{mix} < 0$ kJ/mol and $5\% < \delta < 6.6\%$. The ΔH_{mix}, δ, and ΔS_{mix} of the Ni2.7 and Ni2.1 alloys meet these requirements and form a solid solution of the FCC+B2 phase, as observed experimentally.

A new parameter Ω (Yang and Zhang, 2012) has been proposed to compare the effects of entropy and enthalpy. $\Omega \geq 1.1$ and $\delta \leq 6.6\%$ are considered as the requirements for forming a solid-solution phase. It is clear that the Ω parameters of both alloys are above 1.1.

TABLE 1 | Chemical composition of the $AlCo_xCrFeNi_{3.1-x}$ alloys (at. %).

Alloys	Composition	Al	Cr	Fe	Co	Ni
Ni2.7	Nominal	16.39	16.39	16.39	6.56	44.26
	Actual	15.69	17.02	16.93	6.41	43.94
	A_1	12.72	17.62	19.50	8.22	41.95
	B_1	27.75	9.86	9.30	4.23	48.86
Ni2.1	Nominal	16.39	16.39	16.39	16.39	34.43
	Actual	15.09	17.14	17.03	15.94	34.81
	A_2	10.16	19.94	19.70	18.02	32.17
	B_2	25.51	10.35	11.51	12.63	40.01

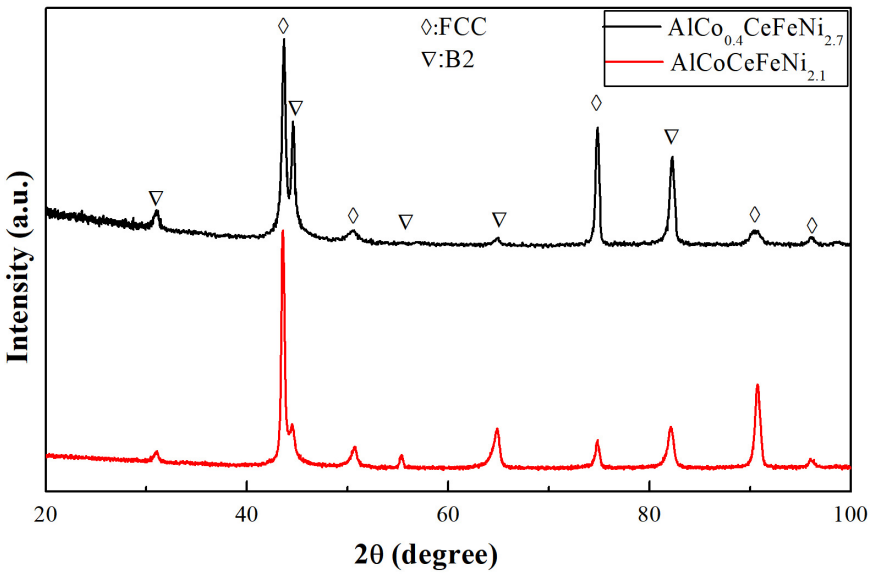

FIGURE 3 | X-ray diffraction (XRD) patterns of the $AlCo_xCrFeNi_{3.1-x}$ alloys.

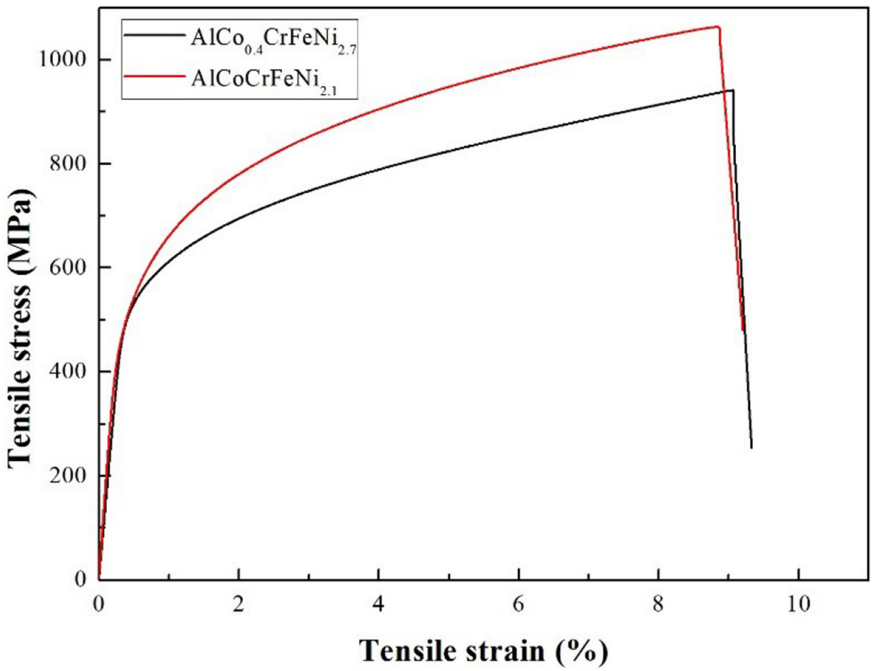

FIGURE 4 | Engineering tensile stress-strain curves of the $AlCo_xCrFeNi_{3.1-x}$ alloys.

Both Co and Ni can promote the formation of the FCC phase (Zhu et al., 2017; Cao et al., 2019). In this work, with decreasing Co and increasing Ni, there was increased FCC phase formation in the Ni2.7 than Ni2.1 alloys. The reason for this could be that the FCC phase formation ability of Ni is stronger than that of Co. Ke et al. (2006) reported that for FCC stabilizers, 1.11 Co is equivalent to 1 Ni, and for BCC stabilizers, 2.23 Cr has the same effect as 1 Al. Therefore, the percentage of Co-FCC in Ni2.7 was ~55.69%, which is slightly larger than in Ni2.1 (55.18%); hence, Ni2.7 has more FCC phase.

Mechanical Properties

According to the experimental results, the yield strengths of the Ni2.7 and Ni2.1 alloys are almost the same. However, the different FCC and B2 phase contents lead to varying fracture strengths and elongations. To be specific, Ni2.7, which contained more of the

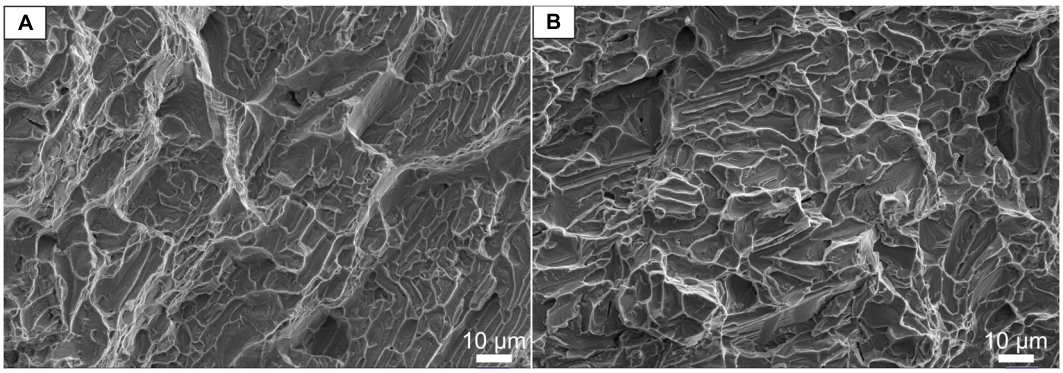

FIGURE 5 | Fracture surface morphology of **(A)** $AlCo_{0.4}CrFeNi_{2.7}$ and **(B)** $AlCoCrFeNi_{2.1}$ at room temperature.

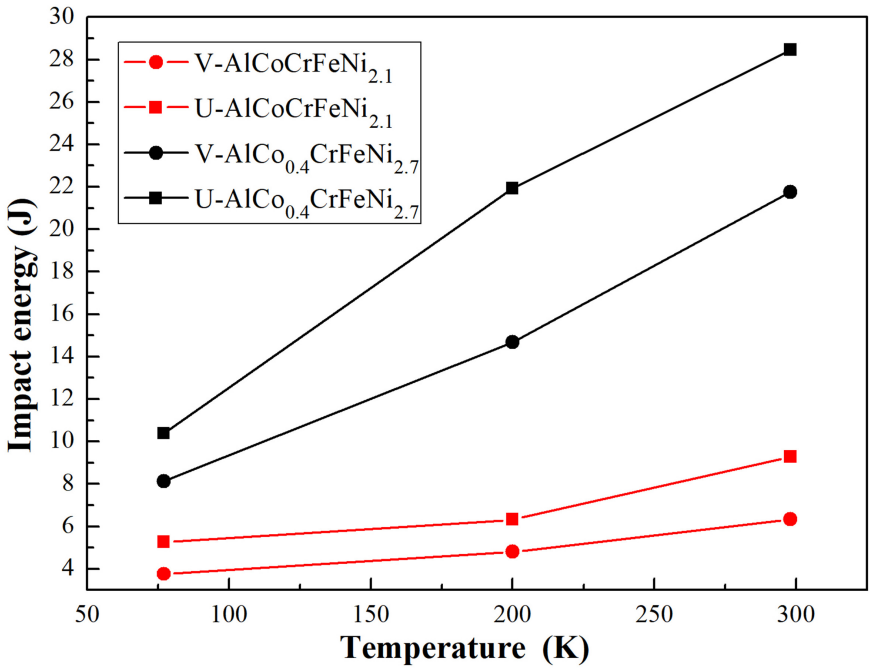

FIGURE 6 | The impact energy as a function of different test temperatures.

TABLE 2 | ΔH_{mix}, δ, ΔS_{mix}, and Ω of the $AlCo_xCrFeNi_{3.1-x}$ alloys.

Alloys	δ (%)	ΔH_{mix} (kJ·mol^{-1})	ΔS_{mix} (J·mol^{-1}·K^{-1})	Ω
$AlCo_{0.4}CrFeNi_{2.7}$	5.17	−12.39	11.89	1.62
$AlCoCrFeNi_{2.1}$	5.17	−11.94	12.89	1.83

FCC phase, showed increased elongation. Similarly, the higher fracture strength of the Ni2.1 alloy was caused by the richer B2 phase inside it.

The presence of the FCC/B2 eutectic structure in the alloys can explain the formation mechanism of the trench-like microstructures (Lu et al., 2017). The B2 phase is hard to deform during the tensile process, while the soft FCC phase could be stretched easily. Then, the FCC phase is necked and gradually thins to form dimples, which gather to form bright lines. The B2 phase is then left at the bottom of the trench and is almost undeformed. From **Figure 5**, it can be seen that the Ni2.7 alloy with more lines composed of dimples has better plasticity.

The impact performance of the two alloys also shows a clear difference. Similar to the tensile test results, the Ni2.7 alloy with the higher FCC phase content has better impact performance. At low temperatures and high strain rates, the difference in the impact toughness between the two alloys is more obvious. The FCC phase content in the Ni2.7 alloy is larger, which may lead to its good impact performance at low temperatures and high strain rates. The results of impact studies on the HEAs are summarized and plotted in **Figure 8A**. The impact properties of the HEAs were relatively dispersed. The impact energy of

$Al_{0·1}CoCrFeNi$, $Al_{0·3}CoCrFeNi$, CoCrFeNi, and CoCrFeMnNi with FCC structures were very high and above 150 J. In addition, phase transformation occurred in CoCrFeNi during the impact process, so it also has an impact energy of ∼100 J. However, the impact energy for the other samples were very low at <10 J. The impact energy values for the Ni2.7 and the Ni2.1 alloys are placed in the mid-region of the data obtained in this work. As the temperature decreased, the impact energy did not change significantly, and the ductile to brittle transition was not observed between 77–298 K.

The relationship between the yield strength and impact energy is shown in **Figure 8B**. The impact energies of $Al_{0·1}CoCrFeNi$ and $Al_{0·3}CoCrFeNi$ exceeded those of most reported metallic materials, while their yield strength was a little lower. In this work, the impact performance of the $AlCo_xCrFeNi_{3.1-x}$ alloys was poor, but it was still better than the AZ91C alloy, Be, Cr, and some carbon steels. In particular, the impact energy of the Ni2.7 alloy was almost equivalent to that of the alloy steel. The yield strength of the $AlCo_xCrFeNi_{3.1-x}$ alloys was higher than most materials (such as low alloy steel, X70 steel, and X80 steel), as shown in **Figure 8B**.

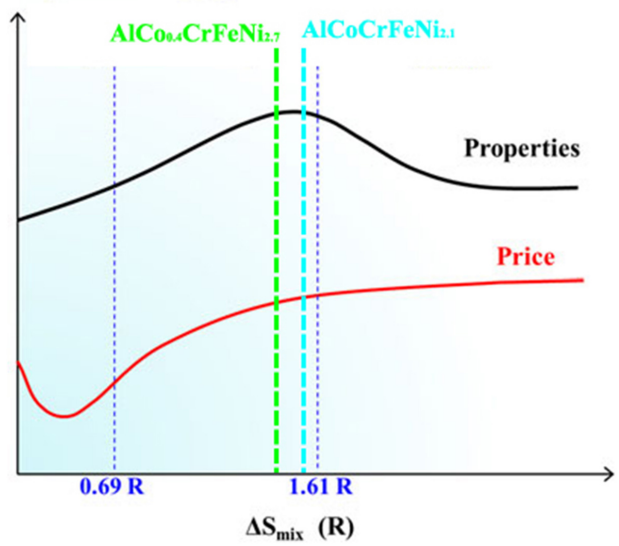

FIGURE 7 | Trend of the properties and price of the $AlCo_xCrFeNi_{3.1-x}$ alloys and other alloys as a function of the entropy.

CONCLUSION

In summary, this work studied the changes in the microstructure and properties of the $AlCo_xCrFeNi_{3.1-x}$ (x = 0.4, 1) alloy on varying the Co and Ni content with the goal of preparing cost-effective alloys. Compared with the perfect eutectic FCC/B2 structure of the $AlCoCrFeNi_{2·1}$ alloy, the $AlCo_{0·4}CrFeNi_{2·7}$ alloy had the structural characteristics of the FCC primary phase and the FCC/B2 eutectic structure. The tensile properties of two alloys were similar, with the FCC phase forming a sharp bright white line when stretched, while the B2 phase was left as a trench with minimal deformation. In terms of the impact performance, the $AlCo_{0·4}CrFeNi_{2·7}$ alloy was much better than the $AlCoCrFeNi_{2·1}$. Additionally, the two alloys did not display characteristics of a ductile-brittle transition within the tested temperature range. Compared with other HEAs, the impact toughness values of the $AlCo_xCrFeNi_{3.1-x}$ alloys were in the middle of the range, and they were far below those of the $Al_{0·3}CoCrFeNi$ and $Al_{0·1}CoCrFeNi$ alloys. Finally, the yield strength of the $AlCo_xCrFeNi_{3.1-x}$ alloys were higher than most of the compared materials.

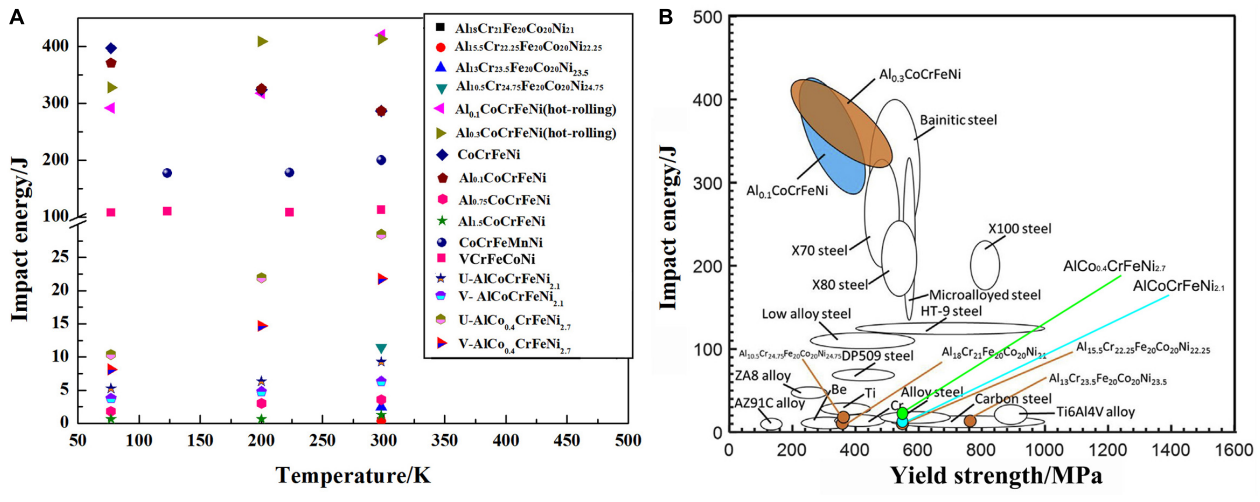

FIGURE 8 | Summary of the impact energy of the materials. **(A)** Impact energies of the $AlCo_xCrFeNi_{3.1-x}$ alloys and other HEAs at the different temperatures (Chen et al., 2016; Li and Zhang, 2016; Kim et al., 2018; Xia et al., 2018; Jo et al., 2019); **(B)** impact energy-yield strength diagram for selected HEAs and some typical materials (Li et al., 2018).

DATA AVAILABILITY STATEMENT

All datasets generated for this study are included in the article/supplementary material.

AUTHOR CONTRIBUTIONS

LZ prepared the high-entropy alloys and wrote the manuscript. YZ offered theoretical guidance. Both authors contributed to the general discussion.

FUNDING

YZ would like to thank the National Natural Science Foundation of China (Grant Nos. 51671020 and 51471025), and the Fundamental Research Funds for the Central Universities (Grant Nos. FRF-MP-19-013 and FEF-MP-18-003) for financial support.

ACKNOWLEDGMENTS

The authors are grateful for support by Professor Lu of Dalian University of Technology for providing the high-entropy alloys.

REFERENCES

Cao, L., Wang, X., Wang, Y., Zhang, L., Yang, Y., Liu, F., et al. (2019). Microstructural evolution, phase formation and mechanical properties of multi-component AlCoCrFeNix alloys. *Appl. Phys. A* 125:699. doi: 10.1007/s00339-019-2959-2950

Chen, C., Pang, S., Cheng, Y., and Zhang, T. (2016). Microstructure and mechanical properties of $Al_{20-x}Cr_{20+0.5x}Fe_{20}Co_{20}Ni_{20+0.5x}$ high entropy alloys. *J. Alloy. Compd.* 659, 279–287. doi: 10.1016/j.jallcom.2015.10.258

Guo, S., and Liu, C. T. (2011). Phase stability in high entropy alloys: formation of solid-solution phase or amorphous phase. *Prog. Nat. Sci.* 21, 433–446. doi: 10.1016/S1002-0071(12)60080-X

Jo, Y. H., Kim, D. G., Jo, M. C., Doh, K. Y., Sohn, S. S., Lee, D., et al. (2019). Effects of deformation–induced BCC martensitic transformation and twinning on impact toughness and dynamic tensile response in metastable VCrFeCoNi high–entropy alloy. *J. Alloy. Compd.* 785, 1056–1067. doi: 10.1016/j.jallcom.2019.01.293

Ke, G. Y., Chen, S. K., Hsu, T., and Yeh, J. W. (2006). FCC and BCC equivalents in as-cast solid solutions of $Al_xCo_yCr_zCu_{0.5}Fe_vNi_w$ high-entropy alloys. *Ann. Chim. Sci. Mat.* 31, 669–683.

Kim, J. H., Lim, K. R., Won, J. W., Na, Y. S., and Kim, H. S. (2018). Mechanical properties and deformation twinning behavior of as-cast CoCrFeMnNi high-entropy alloy at low and high temperatures. *Mater. Sci. Eng. A* 712, 108–113. doi: 10.1016/j.msea.2017.11.081

Li, D., Li, C., Feng, T., Zhang, Y., Sha, G., Lewandowski, J. J., et al. (2017). High-entropy Al0.3CoCrFeNi alloy fibers with high tensile strength and ductility at ambient and cryogenic temperatures. *Acta Mater.* 123, 285–294. doi: 10.1016/j.actamat.2016.10.038

Li, D., and Zhang, Y. (2016). The ultrahigh charpy impact toughness of forged AlxCoCrFeNi high entropy alloys at room and cryogenic temperatures. *Intermetallics* 70, 24–28. doi: 10.1016/j.intermet.2015.11.002

Li, W. D., Liaw, P. K., and Gao, Y. F. (2018). Fracture resistance of high entropy alloys: a review. *Intermetallics* 99, 69–83. doi: 10.1016/j.intermet.2018.05.013

Li, Z., Pradeep, K. G., Deng, Y., Raabe, D., and Tasan, C. C. (2016). Metastable high-entropy dual-phase alloys overcome the strength-ductility trade-off. *Nature* 534, 227–230. doi: 10.1038/nature17981

Liu, X. W., Liu, L., Liu, G., Wu, X. X., Lu, D. H., Yao, J. Q., et al. (2018). The role of carbon in grain refinement of cast CrFeCoNi high-entropy alloys. *Metall. Mater. Trans. A* 49, 2151–2160. doi: 10.1007/s11661-018-4549-8

Lu, Y., Dong, Y., Guo, S., Jiang, L., Kang, H., Wang, T., et al. (2014). A promising new class of high-temperature alloys: eutectic high-entropy alloys. *Sci. Rep.* 4:6200. doi: 10.1038/srep06200

Lu, Y., Gao, X., Jiang, L., Chen, Z., Wang, T., Jie, J., et al. (2017). Directly cast bulk eutectic and near-eutectic high entropy alloys with balanced strength and ductility in a wide temperature range. *Acta Mater.* 124, 143–150. doi: 10.1016/j.actamat.2016.11.016

Lv, Y., Zhao, X., Shi, T., Bai, L., Chen, J., and Wang, X. (2019). Excellent room temperature ductility of as-cast TRIP high-entropy alloy via Mo and C alloying. *J. Mater. Sci.* 55, 2239–2244. doi: 10.1007/s10853-019-04064-9

Manzoni, A., Daoud, H., Volkl, R., Glatzel, U., and Wanderka, N. (2013). Phase separation in equiatomic AlCoCrFeNi high-entropy alloy. *Ultramicroscopy* 132, 212–215. doi: 10.1016/j.ultramic.2012.12.015

Xia, S. Q., Gao, M. C., and Zhang, Y. (2018). Abnormal temperature dependence of impact toughness in AlCoCrFeNi system high entropy alloys. *Mater. Chem. Phys.* 210, 213–221. doi: 10.1016/j.matchemphys.2017.06.021

Yang, X., and Zhang, Y. (2012). Prediction of high-entropy stabilized solid-solution in multi-component alloys. *Mater. Chem. Phys.* 132, 233–238. doi: 10.1016/j.matchemphys.2011.11.021

Yeh, J. W., Chen, S. K., Lin, S. J., Gan, J. Y., Chin, T. S., Shun, T. T., et al. (2004). Nanostructured high-entropy alloys with multiple principal elements: novel alloy design concepts and outcomes. *Adv. Eng. Mater.* 6, 299–303. doi: 10.1002/adem.200300567

Zhang, W., Liaw, P. K., and Zhang, Y. (2018). Science and technology in high-entropy alloys. *Sci. China Mater.* 61, 2–22. doi: 10.1007/s40843-017-9195-9198

Zhang, Y., Yan, X., Ma, J., Lu, Z., and Zhao, Y. (2018). Compositional gradient films constructed by sputtering in a multicomponent Ti–Al–(Cr, Fe, Ni) system. *J. Mater. Res.* 33, 3330–3338. doi: 10.1557/jmr.2018.284

Zhang, Y. (2019). *High-Entropy Materials: A Brief Introduction*. Berlin: Springer. doi: 10.1007/978-981-13-8526-21

Zhang, Y., Zuo, T. T., Tang, Z., Gao, M. C., Dahmen, K. A., Liaw, P. K., et al. (2014). Microstructures and properties of high-entropy alloys. *Prog. Mater. Sci.* 61, 1–93. doi: 10.1016/j.pmatsci.2013.10.001

Zhao, Y. J., Qiao, J. W., Ma, S. G., Gao, M. C., Yang, H. J., Chen, M. W., et al. (2016). A hexagonal close-packed high-entropy alloy: the effect of entropy. *Mater. Des.* 96, 10–15. doi: 10.1016/j.matdes.2016.01.149

Zhu, Z. G., Ma, K. H., Yang, X., and Shek, C. H. (2017). Annealing effect on the phase stability and mechanical properties of (FeNiCrMn)(100-x)Cox high entropy alloys. *J. Alloy. Compd.* 695, 2945–2950. doi: 10.1016/j.jallcom.2016.11.376

Conflict of Interest: The authors declare that the research was conducted in the absence of any commercial or financial relationships that could be construed as a potential conflict of interest.